

PAPER

Helical nanobots as mechanical probes of intra- and extracellular environments

To cite this article: Malay Pal *et al* 2020 *J. Phys.: Condens. Matter* **32** 224001

View the [article online](#) for updates and enhancements.

You may also like

- [Two-photon polymerization-based 4D printing and its applications](#)
Bingcong Jian, Honggeng Li, Xiangnan He et al.
- [Design of nanorobots for exposing cancer cells](#)
Shlomi Dolev, Ram Prasad Narayanan and Michael Rosenblit
- [In situ bending and recovery characterization of hollow glass nanoneedle based on nanorobotic manipulation](#)
Dengfeng Li, Lijun Yang, Wanfeng Shang et al.



WORLD LEADING
MOLECULAR
SPECTROSCOPY SOLUTIONS



edinst.com

Helical nanobots as mechanical probes of intra- and extracellular environments

Malay Pal^{1,6}, Debayan Dasgupta^{1,6}, Neha Somalwar¹, Reshma VR²,
Mayank Tiwari¹, Dharma Teja³, Suma M Narayana⁴, Aradhana Katke⁴,
Jayshree RS⁴, Ramray Bhat^{3,7}, Deepak K Saini^{3,7}
and Ambarish Ghosh^{1,5,7} 

¹ Centre for Nano Science and Engineering, Indian Institute of Science, Bangalore 560012, India

² Center For BioSystems Science And Engineering, Indian Institute of Science, Bangalore 560012, India

³ Department of Molecular Reproduction, Development and Genetics, Indian Institute of Science, Bangalore 560012, India

⁴ Kidwai Memorial Institute of Oncology, Bangalore 560029, India

⁵ Department of Physics, Indian Institute of Science, Bangalore 560012, India

E-mail: ramray@iisc.ac.in, deepaksaini@iisc.ac.in and ambarish@iisc.ac.in

Received 20 November 2019, revised 13 January 2020

Accepted for publication 24 January 2020


Published 3 March 2020



Abstract

A rheological probe that can measure mechanical properties of biological milieu at well-defined locations with high spatial resolution, on a time scale faster than most biological processes, can further improve our understanding of how living systems operate and behave. Here, we demonstrate nanorobots actively driven in realistic *ex vivo* biological systems for fast mechanical measurements with high spatial accuracy. In the various demonstrations of magnetic nanobots as mechanical probes, we report the first direct observation of the internalization of probes by a living cell, the accurate measurement of the ‘fluid phase’ cytoplasmic viscosity of ~200 cP for a HeLa cell, demonstration of intracellular measurements in cells derived from human patients; all of which establish the strength of this novel technique for measurements in both intra- and extracellular environments.

Keywords: intracellular environments, nanorobots, extracellular matrix, microrheology, helical propulsion, viscometry

 Supplementary material for this article is available [online](#)

(Some figures may appear in colour only in the online journal)

Introduction

Biological systems are inherently heterogeneous. As a primary example, one can consider the complex environment inside a living cell, where studying the mechanobiology of the cytoplasm can be challenging due to the dynamic variability of composition inherent in living systems. Cellular architecture is maintained by a dynamic network of protein scaffolds collectively called the cytoskeleton [1], which provides shape to a cell [2], aides in its motility, polarity and

migratory functions. It also plays a crucial role in establishing tissue architecture by establishing inter-cellular and cell-matrix contacts. Outside the cell, secreted fluids provide a constant concentration of moisture, glucose and pH for cellular operations. These extracellular fluids (ECF) are found in body cavities, blood, channels and spaces in the brain and spinal cord, and are spatially contiguous with matrices made of macromolecules like collagen, elastin fibers, glycoproteins, proteoglycans and enzymes, which are collectively known as extracellular matrices (ECMs) [3, 4]. A tissue is a collection of functionally similar cells and their ECMs. In another example, many biological fluids like blood can be considered to be a colloidal suspension of blood cells and platelets

⁶ Equal contributing authors.

⁷ Authors to whom any correspondence should be addressed.

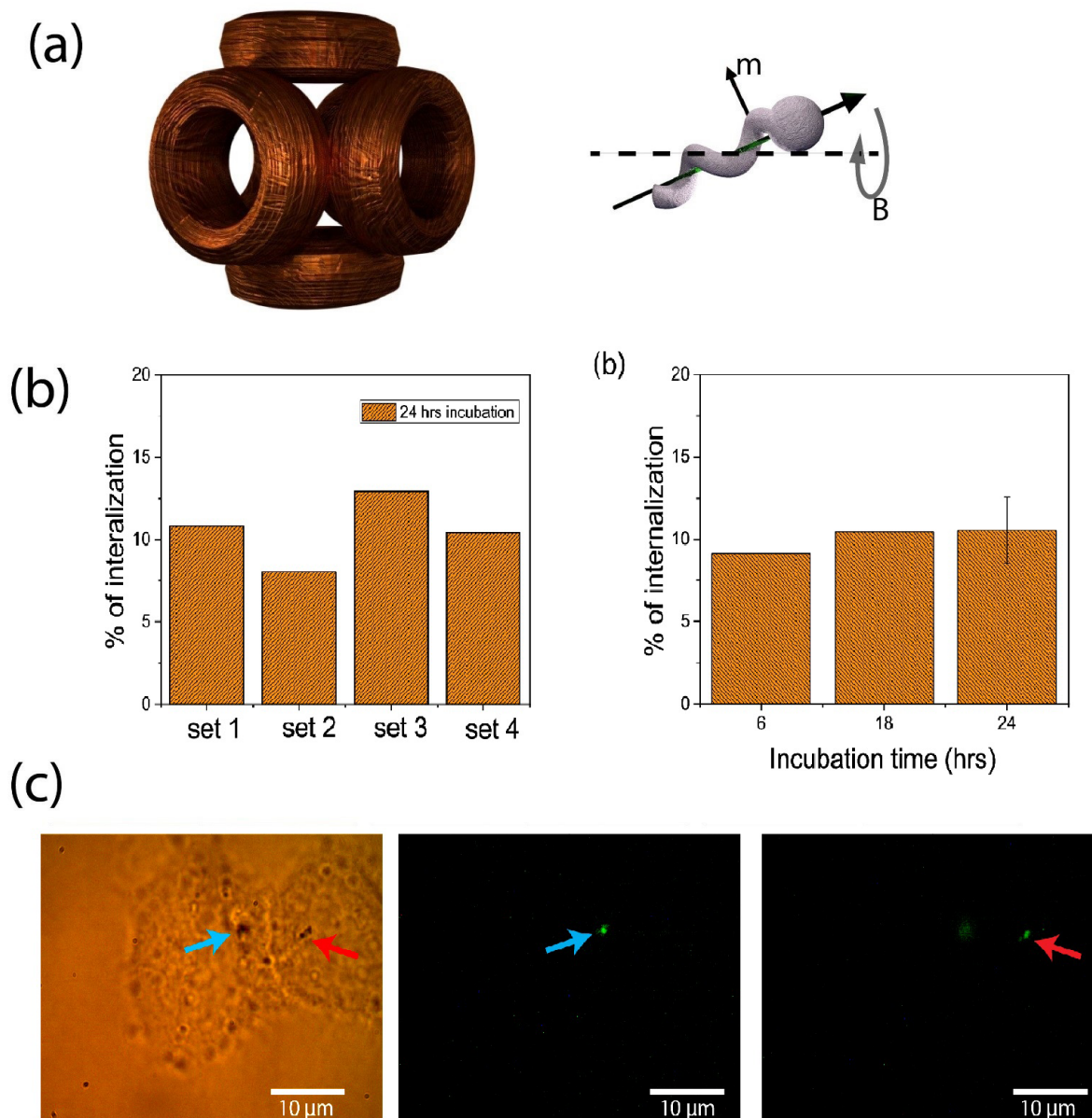


Figure 1. (a) Schematic representation of dynamics of the helical nanorobots in a triaxial Helmholtz coil. The nanorobot has an intrinsic magnetic moment vector denoted by the letter ‘ m ’, which follows the rotating magnetic field ‘ B ’ generated by the coil. (b) Internalization statistics of cells after 24 h and internalization statistics for different incubation times. (c) Brightfield and fluorescent images of 6-aminofluorescein conjugated helical nanobots within living cells.

suspended in plasma proteins and antibodies. Tissues, on the other hand, have densely packed proteinaceous fibers like collagen, with cells suspended in them. They are characterized by long polymer chains with porosity ranging from <200 nm to few microns. The ECM of tissues can exhibit varying degrees of stiffness and elasticity based on the concentration of collagen and elastin. The physical properties of such milieu in the bulk are distinct from those at a micron scale; as a result, bulk rheometers do not capture the myriad of peculiar behavior at local scales that arise due to the complex interplay between the polymer chains that constitute such fluids. Various techniques have been proposed and deployed to study these local heterogeneities. Passive rheology techniques do not require the application of external forces and the response of micron-sized objects to thermal fluctuations can be observed [5]. The most common passive rheology techniques involve light

scattering techniques like dynamic light scattering (DLS) [6], diffusing wave spectroscopy (DWS) [7] and particle tracking microscopy (PTM) [8]. Passive rheology techniques require long measurements to get statistically significant data over reasonable time scales which makes it difficult when the rheological parameters vary quickly, as could be true in various biophysical processes [9–14]. The spatial resolution is limited to the area covered by the fluctuating particle and therefore inherently uncontrolled. Some of these limitations may be overcome in active methods, where an external force is applied to the probe and its response studied. Such techniques are especially useful for characterizing fluids with high viscosity, like most biological fluids, where the position fluctuations of the probes are reduced. Popular active methods involve AFM [15] or manipulation of colloidal probes by optical [16] or magnetic [17] forces.

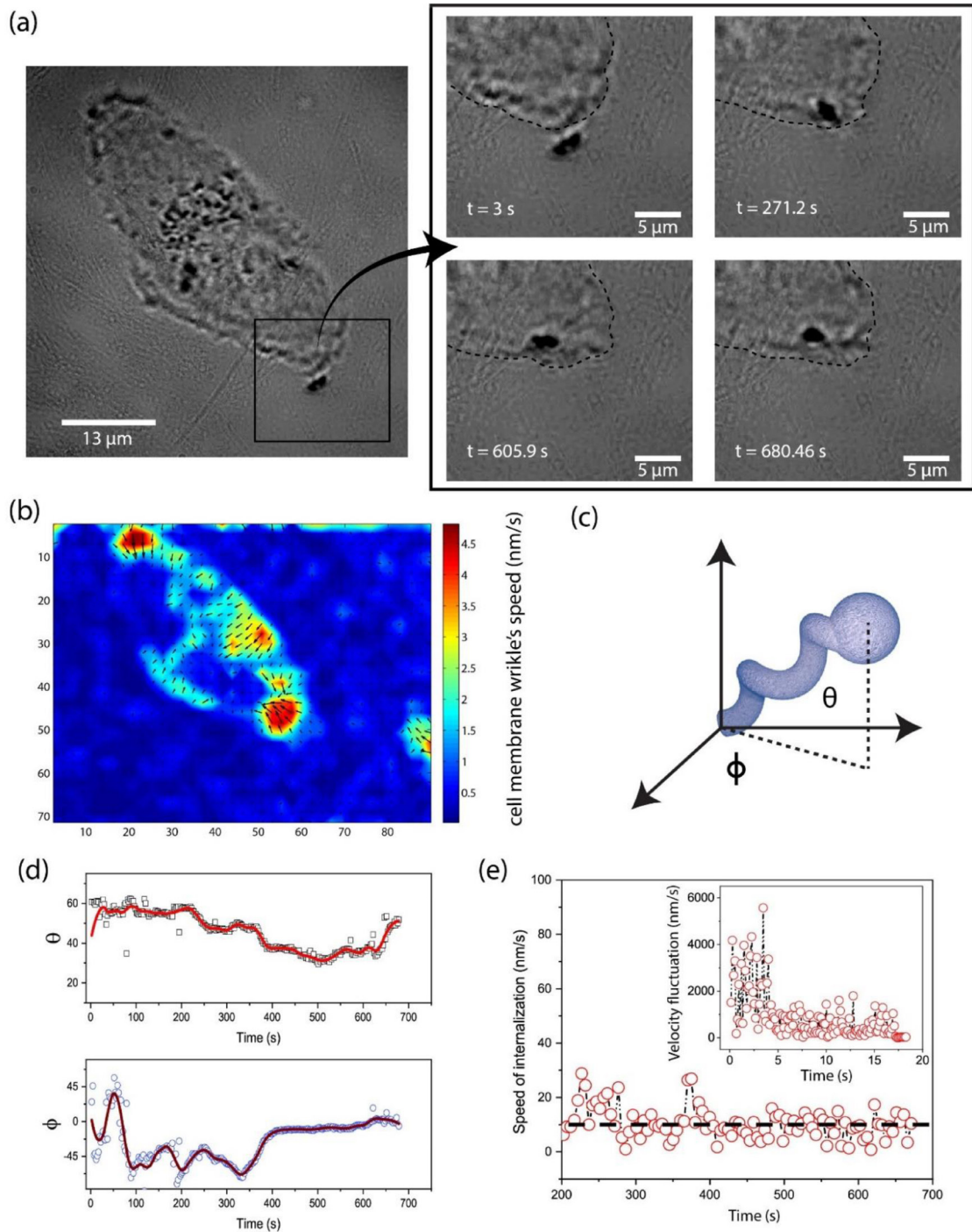


Figure 2. Direct observation of internalization of nanobots by cells. (a) Time lapse image of internalization. (b) Velocimetry analysis of the cell membrane's wrinkles caused during internalization. (c) Schematic showing the orientation angles of a nanorobot. Since under a bright field inverted microscope only a projected 2D image can be observed, the angle θ can be calculated from the projected length and expected length of the helix whereas ϕ can be measured directly from the image. (d) Observed values of the orientation angles during internalization. (e) Speed of internalization. Inset shows velocity fluctuations of the nanorobot during initial 18 s, when it is outside the cell.

The motivation of this paper is to establish the suitability of helical micro and nanorobots, also referred to as micro/nano-motors in the literature, as novel tools for local mechanical measurements in biological media. Past applications of micro/nanobots, driven by various actuation techniques, such as chemical [18–20], optical [21, 22], acoustic [23] and magnetic forces [24–26], cover multiple application domains: targeted drug delivery in biological tissues [19, 27, 28], intracellular

sensing [29] and delivery, environmental remediation [30, 31], microfluidic cargo manipulation [32] and nano-assembly, measurement of local viscosity of model fluids [33] and many more. Among different experimental systems, helical nanorobots driven by rotating magnetic fields [34] deserve special mention because magnetic actuation is minimally invasive to living systems and therefore ideally suited for biological applications. As we show here, this promising system can be

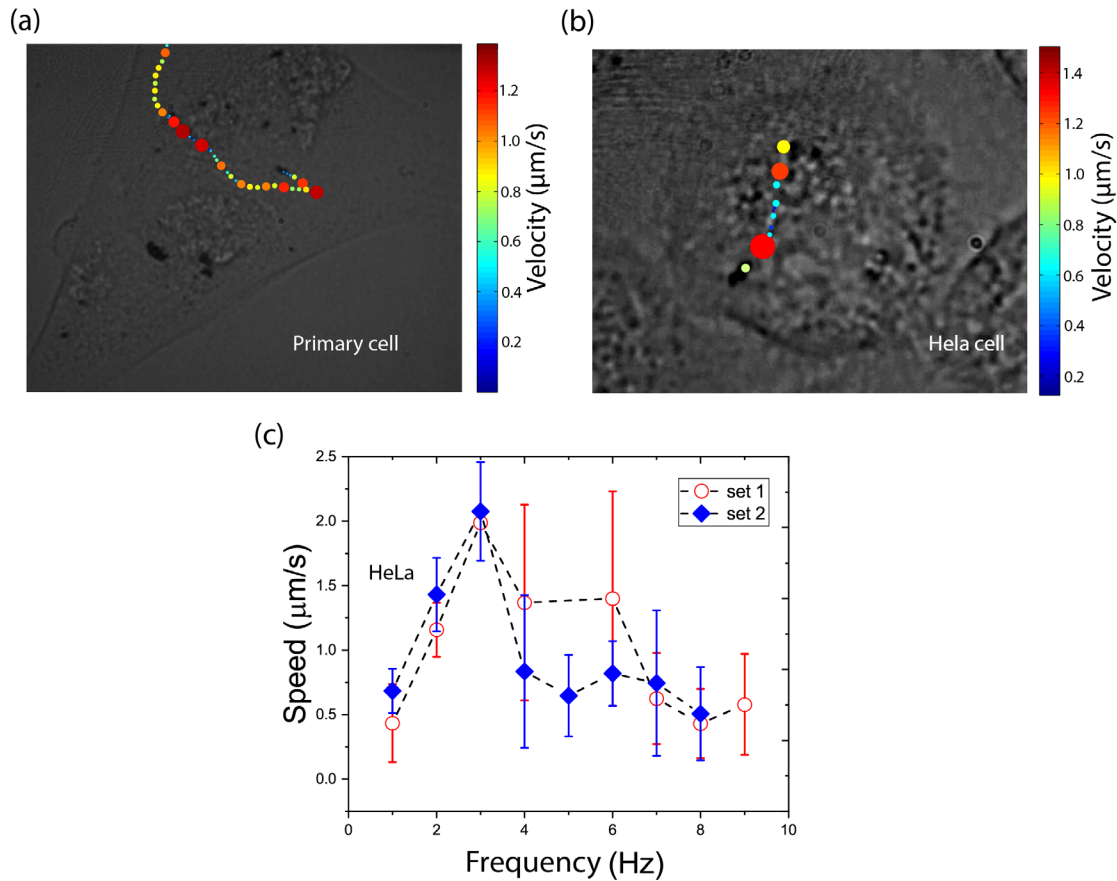


Figure 3. Manipulation of nanobots in cells. (a) Velocity profile of nanorobot inside a primary cell and (b) velocity profile of nanorobot inside a HeLa cell. The colourmaps refer to speed in $\mu\text{m s}^{-1}$. (c) Effective speed of a nanorobot within a cell as a function of frequency of rotating field. Field amplitude: 60 Gauss.

used in highly heterogenous biological environments and in both intra- and extracellular spaces, thus providing a general and powerful tool for biophysical experiments.

In this paper, we first present our studies of internalization of helical nanobots by living cells, including the direct visualization and analysis of these processes. Subsequently, we study their motion inside a living cell to estimate the local mechanical properties of the cytoplasm, including measurements of samples from human cancer patients. As we discuss in detail in the main text, measurements in these complex heterogenous media are fundamentally different from past studies carried out in model fluids such as water, glycerol and silicon oil, necessitating many subtle analyses that have not been considered before. Finally, we show how the same experimental technique can be extended to extracellular matrix-rich environments, as demonstrated here in reconstituted basement membrane (rBM) and gelatin.

Results and discussion

The helical nanorobots were fabricated using glancing angle deposition (GLAD) and described in detail in few of our previous publications [33–35]. Deposition of ferromagnetic material during the helix fabrication ensures formation of a layer of magnetic material inline, protected by a layer of silica. This becomes crucial during actuation in bio-fluids

where the nanorobot should be preferentially inert to the biochemistry of the fluid [27, 33, 35–37]. The experimental setup necessary for maneuvering helical nanorobots is shown in figure 1(a). The dynamics of a helical object under an external rotating magnetic field, in low Reynolds number regime, can be used to measure viscosity of Newtonian as well as shear thinning fluids. In essence, this technique relies on the interaction of a nanorobot as it is moved around in a complex heterogenous environment. The velocity, precession/wobbling angle, the magnetic field amplitude and frequency are continuously monitored to estimate the mechanical properties of the media. A detailed description of the dynamics of our nanorobots has been reported previously and is available as supporting information [33] (see S1 (stacks.iop.org/JPhysCM/32/224001/mmedia)). As noted in the study of the dynamics of the nanorobot, there exists an upper limit of frequency when the velocity of the nanorobot will reach a maximum. Above this frequency, the magnetic moment of the nanorobot will fail to follow the magnetic field resulting in phase slip. This frequency, termed the cutoff frequency can be used for measuring the viscosity of the fluid. Below this frequency, however, the nanorobots exhibit a precessionally (also called wobbling) phase-locked state. Methods by which the viscosity can be gauged from precessing/wobbling motion of the helix have also been described later.

Internalization of helical nanorobots was studied in HeLa cells. Around 0.1 million cells were incubated overnight at 37 °C and 5% CO₂ in a 35 mm glass bottom dish. 10⁶ nanorobots were added into the dish at the start of the experiment and the interaction of the helical microstructures and cells were observed under an inverted bright field microscope.

The percentage of cells with internalized nanorobots was calculated to estimate the gross internalization of these helical structures. A total of 40 fields were randomly imaged throughout the cell culture dish after 24 h of incubation with the nanorobots and the number of cells with at least one internalized nanorobot were counted. We observed 10% ± 2% internalization with respect to the number of cells and the results of the repeated experiments are shown in figure 1(b) (left). The error in internalization percentage is estimated from the standard deviation of internalization percentage of four experiments. The incubation time was altered, and the respective percentage of internalization was recalculated. However, no appreciable change in the percentage of internalization was observed (see figure 1(b) (right)) within this time window. The dependence of internalization on surface properties of the propellers was assessed using fluorescent nanorobots for which the surface was functionalized with 6-aminofluorescein (see figure 1(c)). The functionalization utilized standard method of conjugating the carboxylic acid group on the nanorobots through TEPSA, followed by attachment of the fluorophore using EDC-NHS coupling chemistry. We found that the internalization efficiency of the cells for these fluorescent nanorobots remained the same. Figure 1(c) shows two nanorobots where the bright field image and the corresponding fluorescent images are shown. This experiment suggests that it is possible to incorporate different surface functionalities such as loading drugs [38–41], specific sensing groups [42–45] with the nanorobots, thus opening up new possibilities for intracellular experiments at single cell resolution. As far as we know, some of these functionalities have been demonstrated with ultrasonic nanorobots [46, 47], but not with magnetically driven nanobots.

We now report a direct observation of internalization of nanorobots by a HeLa cell (see figure 2(a)). The nanorobot was observed to execute Brownian motion while outside the cell. On subsequent interaction with the cell membrane, the nanorobot adhered to the membrane and the Brownian motion ceased. The nanorobot was then found to be internalized as can be seen in figure 2(a). While our entire period of observation was close to 10 min, a closer inspection of the movie suggested that process occurred within a time window of 2–5 min. The cell showed an inward flow during the internalization process which was measured by velocimetry algorithm. This was corroborated with the manifestation of wrinkles on the cell surface at the plane of imaging, which is also the plane where the nanorobot resides (see figure 2(b)). We calculated the speed of the formation and deformation of wrinkles using velocimetry algorithm and found it to be maximum around the edges parallel to long axis of the cell and minimum over the edges along the short axis. Maximum speed of the wrinkles was around 5 nm s⁻¹ as shown in the figure 2(b).

Next, we analyzed the orientation of the nanorobot during internalization. The variation in θ and ϕ (see figure 2(d)) confirms that the nanorobot alters its orientations in three dimensions as it gets internalized. The speed of internalization is shown in figure 2(e) where the inset is showing the velocity fluctuation due to Brownian motion when the nanorobot was outside the cell (corresponding to initial 18 s of the movie). Here, we see that the velocity fluctuations are reduced because of interaction of the nanorobot with the cell membrane. The average speed of internalization, as depicted in figure 2(e), was about 10 nm s⁻¹, which is double the speed of deformation of wrinkles on the cell surface (see the supplementary movie).

We demonstrate that it is possible to expand these studies to primary cells from tumor tissues of cervical cancer patients in figure 3(a)). Controlled motion of the nanorobots inside a HeLa cell is demonstrated in figure 3(b) and the average speed of the nanorobot inside the cytosol has been measured (figure 3(c)). Speed fluctuation of nanorobots inside cells is observed for both HeLa and primary cells and the maximum velocities are comparable to the geometrical pitch of the helices (figures 3(a) and (b)) which is in agreement with measurements previously reported [29]. This is surprising considering the hydrodynamic pitch in Newtonian media for these robots which was found to be 180 nm, and therefore implies the presence of strong viscoelasticity [48, 49] within the cell. It is observed that average speed of the nanorobot increases linearly up to a cutoff frequency (figure 3(c)). After the cutoff frequency, 3 Hz in this case, the speed drops due to phase slip of the magnetic moment with the rotating field. The cutoff frequency which can be identified from maximum velocity achieved by the nanorobots is used to calculate the effective viscosity of the cellular cytoplasm. Assuming that the moment vector is aligned to the short axis, the cutoff frequency is described by the equation: $\Omega_2 = \frac{mB}{\gamma_l}$ where m is the magnetic moment of the nanorobot, B is the applied magnetic field and γ_l is the rotational friction coefficient about the long axis. As seen in figure 3(c), Ω_2 has a value of 3 Hz. The magnetic moment of the helix m was $1.3 \times 10^{-15} \text{ A} \cdot \text{m}^2$ and B was 6 mT. With these parameters, we can calculate $\gamma_l = 2.6 \times 10^{-18} \text{ kg} \cdot \text{m}^2 \text{ s}^{-1}$. Given the high aspect ratio of our nanorobot geometry, it can be approximated as a simple rod-like object [50]. The effective viscosity of the media can be calculated, for a rod-like object [51], from the rotation friction coefficient γ_l using the equation: $\gamma_l = \frac{\pi \eta a^3 (1 + C_1)}{0.96 p^2}$ where p is the length to diameter ratio of the rod, $C_1 = \frac{0.677}{p} - 0.183/p^2$. For our nanorobots with $p = 3$, $C_1 = 0.205$ and $a = 3 \mu\text{m}$ the effective viscosity of the cytosol can be calculated to be $\eta = 0.219 \text{ Pa} \cdot \text{s}$ (or 219 cP). Assuming an error of 1 Hz in obtaining the cutoff frequency, the viscosity can be estimated to be between 219 cP (cutoff at 3 Hz) and 274 cP (cutoff at 4 Hz). This error can be substantially reduced if measurements are taken with finer resolution of frequency.

The effective viscosity thus calculated from the velocity of the nanorobot at cutoff frequency indicates that nanorobots can sense a domain of cytoplasmic viscosity. For measuring cytoplasmic viscosity, a distinction is made for smaller probes which do not interact with intracellular macromolecular

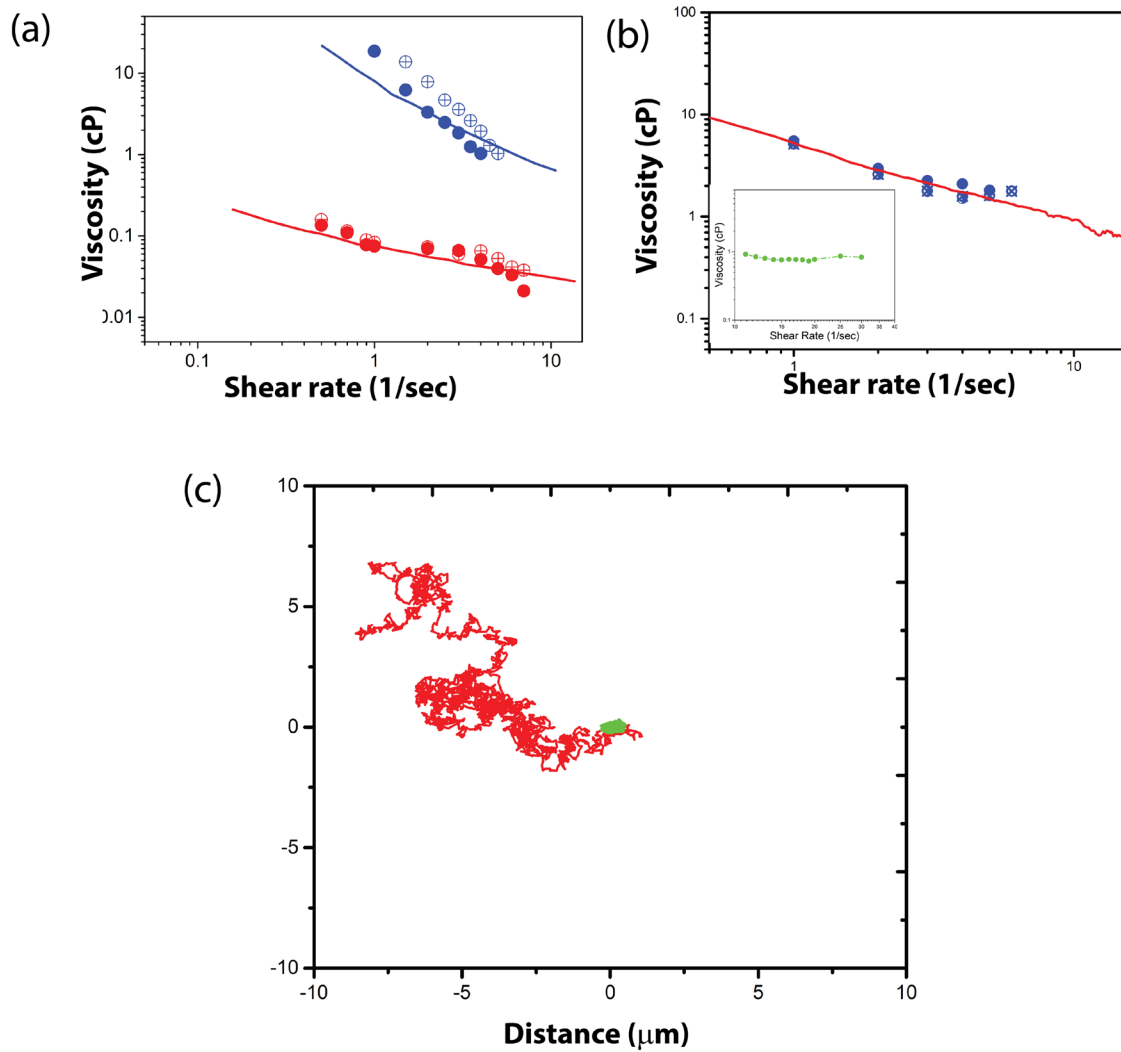


Figure 4. Measurement in gelatin and rBM. (a) Comparison between bulk rheometry (represented by the solid lines) and viscosity sensed by helical nanorobots (represented by the dots) in 2% w/v gelatin (red line and red circles) and 5% w/v gelatin (blue line and blue circles). The open and filled circles represent two measurements done by the same nanorobot in the same fluid. (b) Comparison between passive rheometry (represented by the solid line) and rheology with nanorobot in rBM (represented by the circles) with similar measurements for water in the inset. The curve drawn for passive rheometry was obtained by observing the Brownian motion of a fluorescent bead with a diameter of 200 nm. (c) Trajectory plot (colored red) of a fluorescent bead after injection into rBM shows formation of pockets of water which are ubiquitous when rheological probes are injected into the rBM matrix. This can be compared to the trajectory plot of a bead after ~30 min from the start (colored green).

structures [52]. This is termed the ‘fluid-phase’ cytoplasmic viscosity and various biophysical techniques like fluorescence recovery after photobleaching (FRAP) [53, 54] and passive diffusion [55] have been used to calculate this number. Values ranging from 2 cP to > 100 cP have been reported for various cells. For HeLa cells intracellular viscosities in the range $0.05\text{--}0.2 \text{ Pa} \cdot \text{s}$ has been reported [56–58]. Experiments with micron-sized wires also provide similar range of viscosity [59]. Our calculated value is in good agreement with previously reported values. The length scale of the rheological probe becomes important due to the existence of various relevant length scales within the cytoplasm arising from the inherent anisotropies and porosities of the intracellular environment. Accordingly, the measurements are expected to be subjected to strong steric effects depending on the relative dimensions of our helical probes and the fluidic pockets through which the nanorobots are driven.

Till now we have demonstrated how the cutoff frequency can be used to gauge the viscosity in a densely packed environment like the cytoplasm. In our previous work, we had also demonstrated how the changes in dynamics of the helical nanorobot in response to the viscosity of the media is also manifest in its precession angle. At suitable values of actuating frequency Ω_B (expressed in Hz), the nanorobot starts to precess about the axis of the field rotation and the angle of precession can be observed experimentally. Measurement of the precession angle can lead to an estimation of the local viscosity as discussed later. We tried to drive the nanorobot to its precessional phase-locked state while inside the cell; however, tumbling or wobbling of the nanorobot was never observed during our experiments. We believe this can be due to the densely packed, crowded environment inside the cells which restricts the degrees of freedom for the movement of the nanorobot. However, precessional motion of nanorobots

was observed during our experiments for mechanical investigation of the extracellular matrix.

The dynamics of the nanorobot in its precessional phase locked can be described as follows: precession angle, denoted as α_p , can be measured experimentally using standard bright field microscopy which relate viscosity of the surrounding media by the following equation [33]:

$$\eta = \frac{m B \sin(\theta_m)}{2\pi \Omega_B f_s \sin(\alpha_p)}.$$

Here, m is the magnetic moment of the structure, B and Ω_B are strength and frequency of applied field, θ_m is the magnetization angle as shown in the figure 1(b), f_s is a geometrical factor. The precessional phase locked motion continues until Ω_2 . Due to the ability of precise spatial manipulation and a length scale of few microns, it can probe the heterogeneity in surrounding fluid with a resolution comparable to the body length.

The experimental measurement of $\eta(\gamma)$ in biofluids for a range of actuating frequencies are shown in figure 4(a). The shear-thinning property of gelatin at different concentrations is evident from the data. The slope of shear-dependent viscosity is found to be in good agreement with the data obtained from bulk rheometry [60]. Since the actual value of ' m ' is not known for the individual nanorobot, it was kept adjustable for the analysis. In principle, this value can be obtained from a self-referenced measurement where the nanorobot is driven from a fluid of known viscosity to the fluid where the measurement is to be done. Also note that the typical values of m for nanorobots fabricated during the same evaporation run are expected to lie within a certain range [33] which depend on size, configuration and properties of the magnetic material. The field of actuation was kept at 60 G and 70 G during which the frequency was changed from 0.1 Hz to 10 Hz. The actuating frequency is assumed to be the same as the shear rate. Any scaling that may have been necessary has been corrected by the adjustable parameter m .

The experimental data plotted in figure 4(b) for reconstituted basement membrane matrix (rBM) shows a similar shear dependence, i.e. shear thinning behavior. The rBM used here was diluted with water 2:1 (water:rBM) v/v to reduce the viscous drag on the rheological probes. However, introduction of rheological probes gives rise to short-term temporal inhomogeneities. This happens because the media in which the probes like beads or nanorobots are suspended do not necessarily mix with the gelatinous matrix of the rBM. For our experiments, it was observed that the very act of introducing rheological probes into the bulk of the fluid creates local inhomogeneities that persist over a time scale of few minutes. As shown in figure 4(c), the trajectory of a fluorescent bead, 6 min after injection into rBM is shown in red. The entire duration for the red trajectory plot is 4 min, during which the bead shows a much larger spread of random walk. However, the green trajectory is the random walk executed by another bead almost 30 min after the start of experiment. The spread of the bead is contained to a much smaller region for the same duration of 4 min. This indicates that the introduction of rheological

probes can create localized 'puddles' of fluids where the process of mixing is not complete. A rheological probe, whose ability to sense spatial heterogeneity at a rate faster than the mixing time scale can provide such dynamic information. As demonstrated by the trajectory plot in figure 4(c), the net Brownian motion of the bead rapidly decreases from the time of injection of the probes into the rBM before stabilizing. We have also measured viscosity of water as a function of shear rate, which shows Newtonian behavior at the first place and helps us compare the shear thinning behavior of rBM. This data is shown in the inset of figure 4(b). The demonstration of viscometry in rBM is of interest as bulk rheology for rBM is cost prohibitive and unable to capture the local heterogeneities of the fluid.

As mentioned earlier, the nanorobots can measure viscosity much faster than conventional passive bead-based microrheology, making it useful for the cases where viscosity of the medium changes faster than the time scales usually associated with passive micro rheology measurements [13, 14]. Such a scenario is ubiquitous in experiments with bio-fluids which are heterogeneous and where changes can occur at various time scales, depending on chemical kinetics and temperature among other external factors.

Conclusion

We demonstrated how active probes such as a maneuverable nanorobots may be used for local viscometry on fluids of biological significance. We presented evidence of internalization of such nanorobots by cells, which is crucial to establish this novel tool for intracellular measurement. Measurement of viscosity from the highest velocity achieved at a cutoff frequency was shown to be in good agreement with previously reported values. Different strategies for intracellular and extracellular measurement seem to be strongly dependent on the crowding of the local environment. While measuring the cutoff frequency was best suited for a packed environment like the interior of a cell, dynamical methods proved to be effective for ECF like the rBM matrix. Overall, helical nanorobots are a promising new tool for getting real time mechanical data from live systems and their surrounding microenvironments, while being minimally invasive and tracking fast temporal changes in fluids with large spatial heterogeneity. The unique ability of the helical nanorobots to be accurately driven to a desired site for probing can be useful for studying site-specific changes like the transformations happening at the edges of a cytoplasm during cell migration or the local physical changes near the cell membrane during cellular uptake of food or certain drugs. Since the nanorobots can be driven through the interface of two miscible fluids, self-referenced and therefore highly quantitative measurements are possible with such systems, where properties of the test fluid are measured in reference to the properties of a well-characterized fluid. Such possibilities may be used to answer fundamental questions about local rheological changes happening

in tandem inside cells or their environments due to various bio-physiochemical processes.

Materials and methods

Fabrication of nanorobots

The helical nanorobots were fabricated on a patterned silicon wafer using a physical vapor deposition technique called GLAD. For patterning, a monolayer of $0.73\ \mu\text{m}$ polystyrene beads was made on silicon wafer using Langmuir Blodgett technique. The diameter of the beads was reduced using plasma etching to $0.5\ \mu\text{m}$. The beads were then used as a mask to etch the silicon wafer using reactive-ion etching to form silicon pillars. Nanorobots were grown on this patterned wafer using GLAD where the vapour falls on the pattern at an extreme angle ($\sim 5^\circ$). The shadowing effect combined with controlled rotation of the wafer results in the formation of helical structures. Silica was deposited in-line with a ferromagnetic material. For viscosity measurements, nanorobots of length $3\ \mu\text{m}$ and $1\ \mu\text{m}$ pitch was fabricated on 200 nm diameter silicon pillars and 50 nm of iron-cobalt (1:3) was used as ferromagnetic material. In case of experiments in cells, nanorobots of length $3\ \mu\text{m}$ and $1.7\ \mu\text{m}$ pitch was fabricated on 400 nm diameter silicon pillars and 50 nm of iron was used as ferromagnetic material.

Preparation of matrigel and gelatin solution

Matrigel: $50\ \mu\text{l}$ of thawed Corning Matrigel was placed on a clean glass slide using pre-cooled pipette and allowed to gel in room temperature. After the gelation of the Matrigel matrix, $10\ \mu\text{l}$ nanorobot solution in DI (de-ionized) water was injected into the matrix

Gelatin: 0.2 g of gelatin powder was mixed with 10 ml of DI water to prepare the 2% w/v concentration of gelatin. The mixture was placed in a water bath maintained at 60°C for 15 min . The solution was allowed to cool down to room temperature. $10\ \mu\text{l}$ of nanorobot solution in DI water was added to this solution.

Preparation of fluorescent nanorobots

The wafer containing nanorobots was cleaned using plasma cleaner for 15 min . The cleaned wafer was transferred to 200 mM TEPSA solution in DMF containing DI water, and TBAH in 1:1 ratio and heated at 120°C overnight in a water bath. The wafer was washed with DMF and DI water. The wafer was then transferred to a solution containing 10 mg each of 6-aminofluorescein, EDC, NHS and $500\ \mu\text{l}$ each of DMSO and MES buffer and kept on a rocker in dark for 24 h . The wafer was finally washed with PBS and sonicated in DI water to obtain fluorescent nanorobots in solution.

Cell culture

HeLa cells (ATCC, USA) were grown in DMEM supplemented with 10% FBS at 37°C and 5% CO_2 . 0.1 million cells were

grown overnight in 35 mm glass bottom dishes and incubated with 10^6 fluorescent nanorobots for 24 h in culture medium.

Acknowledgments

We thank DBT (DBTO0525) and RGUHS for funding. This work was partially supported by DST, Government of India. We also thank MHRD, MeitY, and DST for supporting the facilities at Centre for Nano Science and Engineering, Indian Institute of Science. MP thanks CSIR for PhD fellowship. RB would like to acknowledge support from the SERB ECR Grant (1586).

ORCID iDs

Ambarish Ghosh  <https://orcid.org/0000-0002-2524-0014>

References

- [1] Fletcher D A and Mullins R D 2010 Cell mechanics and the cytoskeleton *Nature* **463** 485–92
- [2] Cooper G M 2000 *The Cell: a Molecular Approach* (Sunderland, MA: Sinauer Associates)
- [3] Theocharis A D, Skandalis S S, Gialeli C and Karamanos N K 2016 Extracellular matrix structure *Adv. Drug Deliv. Rev.* **97** 4–27
- [4] Lo C M, Wang H B, Dembo M and Wang Y L 2000 Cell movement is guided by the rigidity of the substrate *Biophys. J.* **79** 144–52
- [5] Waigh T A 2005 Microrheology of complex fluids *Rep. Prog. Phys.* **68** 685–742
- [6] Berne B J and Pecora R 2000 *Dynamic Light Scattering: with Applications to Chemistry, Biology, and Physics* (New York: Dover)
- [7] Pine D J, Weitz D A, Chaikin P M and Herbolzheimer E 1988 Diffusing wave spectroscopy *Phys. Rev. Lett.* **60** 1134–7
- [8] Mason T G, Ganesan K, van Zanten J H, Wirtz D and Kuo S C 1997 Particle tracking microrheology of complex fluids *Phys. Rev. Lett.* **79** 3282–5
- [9] Chen D 2010 Microrheology of soft matter *Publicly Access. Penn Dissertations*
- [10] Levine A J and Lubensky T C 2001 Response function of a sphere in a viscoelastic two-fluid medium *Phys. Rev. E* **63** 041510
- [11] Squires T M 2008 Nonlinear microrheology: bulk stresses versus direct interactions *Langmuir* **24** 1147–59
- [12] Squires T M and Brady J F 2005 A simple paradigm for active and nonlinear microrheology *Phys. Fluids* **17** 073101
- [13] Tassieri M 2015 Linear microrheology with optical tweezers of living cells ‘is not an option’! *Soft Matter* **11** 5792–8
- [14] Tassieri M 2019 Microrheology with optical tweezers: peaks and troughs. *Curr. Opin. Colloid Interface Sci.* **43** 39–51
- [15] Mahaffy R E, Shih C K, MacKintosh F C and Käs J 2000 Scanning probe-based frequency-dependent microrheology of polymer gels and biological cells *Phys. Rev. Lett.* **85** 880–3
- [16] Ashkin A, Dziedzic J M, Bjorkholm J E and Chu S 1986 Observation of a single-beam gradient force optical trap for dielectric particles *Opt. Lett.* **11** 288
- [17] Ziemann F, Rädler J and Sackmann E 1994 Local measurements of viscoelastic moduli of entangled actin networks using an oscillating magnetic bead microrheometer *Biophys. J.* **66** 2210–6

- [18] Li J *et al* 2016 Enteric micromotor can selectively position and spontaneously propel in the gastrointestinal tract *ACS Nano* **10** 9536–42
- [19] Gao W *et al* 2015 Artificial micromotors in the mouse's stomach: a step toward *in vivo* use of synthetic motors *ACS Nano* **9** 117–23
- [20] Dey K K *et al* 2015 Micromotors powered by enzyme catalysis *Nano Lett.* **15** 8311–5
- [21] Zhou C, Zhang H P, Tang J and Wang W 2018 Photochemically powered AgCl janus micromotors as a model system to understand ionic self-diffusiophoresis *Langmuir* **34** 3289–95
- [22] Ghosh S and Ghosh A 2019 All optical dynamic nanomanipulation with active colloidal tweezers *Nat. Commun.* **10** 4191
- [23] Wang W, Castro L A, Hoyos M and Mallouk T E 2012 Autonomous motion of metallic microrods propelled by ultrasound *ACS Nano* **6** 6122–32
- [24] Ghosh A, Paria D, Singh H J, Venugopalan P L and Ghosh A 2012 Dynamical configurations and bistability of helical nanostructures under external torque *Phys. Rev. E* **86** 1–5
- [25] Mandal P, Patil G, Kakoty H and Ghosh A 2018 Magnetic active matter based on helical propulsion *Acc. Chem. Res.* **51** 2689–98
- [26] Mandal P, Chopra V and Ghosh A 2015 Independent positioning of magnetic nanomotors *ACS Nano* **9** 4717–25
- [27] Wu Z *et al* 2018 A swarm of slippery micropropellers penetrates the vitreous body of the eye *Sci. Adv.* **4** eaat4388
- [28] Venugopalan P L, Jain S, Shivashankar S and Ghosh A 2018 Single coating of zinc ferrite renders magnetic nanomotors therapeutic and stable against agglomeration *Nanoscale* **10** 2327–32
- [29] Pal M *et al* 2018 Maneuverability of magnetic nanomotors inside living cells *Adv. Mater.* **30** 1800429
- [30] Parmar J, Vilela D, Villa K, Wang J and Sánchez S 2018 Micro- and nanomotors as active environmental microcleaners and sensors *J. Am. Chem. Soc.* **140** 9317–31
- [31] Zarei M and Zarei M 2018 Self-propelled micro/nanomotors for sensing and environmental remediation *Small* **14** 1800912
- [32] Ghosh S and Ghosh A 2018 Mobile nanotweezers for active colloidal manipulation *Sci. Robot.* **3** eaaq0076
- [33] Ghosh A *et al* 2018 Helical nanomachines as mobile viscometers *Adv. Funct. Mater.* **28** 1705687
- [34] Ghosh A and Fischer P 2009 Controlled propulsion of artificial magnetic nanostructured propellers *Nano Lett.* **9** 2243–5
- [35] Ghosh A, Mandal P, Karmakar S and Ghosh A 2013 Analytical theory and stability analysis of an elongated nanoscale object under external torque *Phys. Chem. Chem. Phys.* **15** 10817–23
- [36] Venugopalan P L *et al* 2014 Conformal cytocompatible ferrite coatings facilitate the realization of a nanovoyager in human blood *Nano Lett.* **14** 1968–75
- [37] Schamel D *et al* 2014 Nanopropellers and their actuation in complex viscoelastic media *ACS Nano* **8** 8794–801
- [38] de Ávila B E-F *et al* 2017 Micromotor-enabled active drug delivery for *in vivo* treatment of stomach infection *Nat. Commun.* **8** 272
- [39] Gao W and Wang J 2014 Synthetic micro/nanomotors in drug delivery *Nanoscale* **6** 10486–94
- [40] Wang L *et al* 2016 Self-propelled manganese oxide-based catalytic micromotors for drug delivery *RSC Adv.* **6** 65624–30
- [41] Wu Z *et al* 2015 RBC micromotors carrying multiple cargos towards potential theranostic applications *Nanoscale* **7** 13680–6
- [42] Jurado-Sánchez B and Escarpa A 2017 Janus micromotors for electrochemical sensing and biosensing applications: a review *Electroanalysis* **29** 14–23
- [43] Patino T *et al* 2019 Self-sensing enzyme-powered micromotors equipped with pH-responsive DNA nanoswitches *Nano Lett.* **19** 3440–7
- [44] Gao W, D'Agostino M, Garcia-Gradilla V, Orozco J and Wang J 2013 Multi-fuel driven Janus micromotors *Small* **9** 467–71
- [45] Karshalev E, Esteban-Fernández de Ávila B and Wang J 2018 Micromotors for 'Chemistry-on-the-Fly' *J. Am. Chem. Soc.* **140** 3810–20
- [46] Wang W *et al* 2014 Acoustic propulsion of nanorod motors inside living cells *Angew. Chem., Int. Ed. Engl.* **53** 3201–4
- [47] Esteban-Fernández de Ávila B *et al* 2017 Nanomotor-enabled pH-responsive intracellular delivery of caspase-3: toward rapid cell apoptosis *ACS Nano* **11** 5367–74
- [48] Spagnolie S E, Liu B and Powers T R 2013 Locomotion of helical bodies in viscoelastic fluids: enhanced swimming at large helical amplitudes *Phys. Rev. Lett.* **111** 068101
- [49] Purcell E M, Powers T R and Breuer K S 1997 The efficiency of propulsion by a rotating flagellum *Proc. Natl Acad. Sci. USA* **94** 11307–11
- [50] Constantino M A, Jabbarzadeh M, Fu H C and Bansil R 2016 Helical and rod-shaped bacteria swim in helical trajectories with little additional propulsion from helical shape *Sci. Adv.* **2** e1601661
- [51] Ortega A and García de la Torre J 2003 Hydrodynamic properties of rodlike and disklike particles in dilute solution *J. Chem. Phys.* **119** 9914–9
- [52] Bicknese S, Periasamy N, Shohet S B and Verkman A S 1993 Cytoplasmic viscosity near the cell plasma membrane: measurement by evanescent field frequency-domain microfluorimetry *Biophys. J.* **65** 1272–82
- [53] Swaminathan R, Bicknese S, Periasamy N and Verkman A S 1996 Cytoplasmic viscosity near the cell plasma membrane: translational diffusion of a small fluorescent solute measured by total internal reflection-fluorescence photobleaching recovery *Biophys. J.* **71** 1140–51
- [54] Swaminathan R, Hoang C P and Verkman A S 1997 Photobleaching recovery and anisotropy decay of green fluorescent protein GFP-S65T in solution and cells: cytoplasmic viscosity probed by green fluorescent protein translational and rotational diffusion *Biophys. J.* **72** 1900–7
- [55] Mastro A M, Babich M A, Taylor W D and Keith A D 1984 Diffusion of a small molecule in the cytoplasm of mammalian cells *Proc. Natl Acad. Sci. USA* **81** 3414–8
- [56] Berret J-F 2016 Local viscoelasticity of living cells measured by rotational magnetic spectroscopy *Nat. Commun.* **7** 10134
- [57] Kuimova M K *et al* 2009 Imaging intracellular viscosity of a single cell during photoinduced cell death *Nat. Chem.* **1** 69–73
- [58] Kuimova M K, Yahioglu G, Levitt J A and Suhling K 2008 Molecular rotor measures viscosity of live cells via fluorescence lifetime imaging *J. Am. Chem. Soc.* **130** 6672–3
- [59] Chevy L, Colin R, Abou B and Berret J-F 2013 Intracellular micro-rheology probed by micron-sized wires *Biomaterials* **34** 6299–305
- [60] Harman M W *et al* 2012 The heterogeneous motility of the Lyme disease spirochete in gelatin mimics dissemination through tissue *Proc. Natl Acad. Sci. USA* **109** 3059–64